Int. J. Heat Mass Transfer. Vol. 32, No. 3, pp. 551–562, 1989
Printed in Great Britain

0017–9310/89 $3.00 + 0.00
Pergamon Press plc

Fluid flow and heat transfer in an axially rotating pipe—I. Effect of rotation on turbulent pipe flow

G. REICH and H. BEER

Institut für Technische Thermodynamik, Technische Hochschule Darmstadt,
Petersenstrasse 30, 6100 Darmstadt, Federal Republic of Germany

(*Received* 11 *May* 1988)

Abstract—The effects of tube rotation on the velocity and temperature distribution, on the friction coefficient and on the heat transfer to a fluid flowing inside a tube are examined experimentally and by analysis. Rotation is found to have a very marked influence on the suppression of the turbulent motion because of radially growing centrifugal forces. The analytical study is performed for flow and heat transfer in an axially rotating pipe by applying a modified mixing length theory to a fully developed turbulent pipe flow with superimposed rotation. To express the degree of turbulence suppression, due to the centrifugal forces, the mixing length is modified by a function of the Richardson number Ri. The theoretical results are compared with the experimental findings.

1. INTRODUCTION

FLUID flow and heat transfer in rotating systems are not only of considerable theoretical interest, but also of great practical importance. Transport phenomena in rotating systems, therefore, have challenged engineers and scientists for a long time. In 1917 Lord Rayleigh [1] investigated the dynamics and stability of revolving fluids. Also, some of the classical solutions of the Navier–Stokes and conservation of energy equations were obtained for rotating systems. Von Kármán [2] investigated the flow induced by a rotating disk and the associated convective heat transfer in 1921. The fluid mechanics stability criteria for circular flow in an annulus formed between two concentric rotating cylinders were studied by Taylor [3]. Problems such as free convection from a rotating cylinder, flow normal to a rotating cylinder, flow about a rotating disk, and flow in rotating annuli have been treated both, analytically and by experiment in considerable detail.

Another rather elementary and common rotating configuration, which is the subject of this paper, is the case of flow through a rotating pipe. The obvious technical application is a rotating power transmission shaft that is longitudinally bored, and through which a fluid is pumped for cooling or for other purposes. The objective of this paper is to present the results of an experimental and theoretical study of the fluid flow and the heat transfer in an axially rotating pipe.

When a fluid enters a pipe rotating about its axis, tangential forces acting between the rotating pipe and the fluid cause the fluid to rotate with the pipe, resulting in a flow pattern rather different from that observed in a non-rotating pipe. Rotation was found to have a very marked influence on the suppression of the turbulent motion because of radially growing centrifugal forces.

The effects of pipe rotation on the hydraulic loss have been investigated experimentally by Levy [4], White [5] and Shchukin [6]. If the flow is initially turbulent, the pressure loss decreases with increasing rotational speed. For turbulent flows in a rotating pipe, Borisenko *et al.* [7] studied the effect of rotation on the turbulent velocity fluctuations using hot-wire probes and showed that they were suppressed by the rotation. Murakami and Kikuyama [8] measured the time-mean velocity components and hydraulic losses in an axially rotating pipe when a fully developed turbulent flow was introduced into the pipe. The pipe rotation was found to suppress the turbulence in the flow, and also to reduce the hydraulic loss. With increasing rotational speed the axial velocity distribution finally approaches the Hagen–Poiseuille flow. More recently Kikuyama *et al.* [9] measured the time-mean velocities and turbulent fluctuations inside the turbulent boundary layers which developed in an axially rotating pipe in the case of an undeveloped flow with a rectangular axial velocity distribution being introduced in the pipe. The pipe rotation yielded two counter effects on the flow: a destabilizing effect due to a large shear stress caused by the rotating pipe wall near the inlet region of the rotating pipe, and a stabilizing effect due to the centrifugal force of the tangential velocity component of the flow, which becomes dominant in the downstream sections. Nishibori *et al.* [17] investigated experimentally the flow in the inlet region of an axially rotating pipe when fully developed flow was introduced into it. A laminarization phenomenon was observed in the developing rotating layer, which has been found to be more pronounced in the inlet region where a non-rotating inner core exists. By use of a modified mixing length theory for the turbulent pipe flow, Kikuyama *et al.* [10] calculated velocity distributions and friction coefficients in the fully developed region of a rotating

NOMENCLATURE

c_p	specific heat at constant pressure
D	pipe diameter
F	auxiliary function
k	thermal conductivity
k_t	turbulent thermal conductivity
L	pipe length
l, l_q	hydrodynamic and thermal mixing length in the rotating pipe
l_0, l_{q0}	hydrodynamic and thermal mixing length in the non-rotating pipe
N	rotation rate
Nu	Nusselt number
Pr	Prandtl number
Pr_t	turbulent Prandtl number
p	pressure
$\dot{q}$	heat flux density
$\dot{q}_{rw}$	heat flux density at the pipe wall
R	pipe radius
Re	flow-rate Reynolds number
Re_ϕ	rotational Reynolds number
Re_*	Reynolds number based on the friction velocity
Ri	Richardson number
r	coordinate in the radial direction
$\tilde{r}$	dimensionless coordinate in the radial direction
T	time-mean temperature
T'	temperature fluctuation
t	time
v_r, v_ϕ, v_z	time-mean velocity in the radial, tangential, and axial directions
$v_{\phi w}$	tangential velocity of the pipe wall
$\tilde{v}_z$	dimensionless axial velocity
$\bar{v}_z$	mean axial velocity over the pipe cross-section
$\tilde{\bar{v}}_z$	dimensionless mean axial velocity
v_t'	velocity fluctuation
v_*	friction velocity
y^+	dimensionless radial distance from the pipe wall
z	coordinate in the axial direction
$\tilde{z}$	dimensionless coordinate in the axial direction.

Greek symbols

ε	truncation criterion
$\varepsilon_\tau, \varepsilon_q$	eddy diffusivity for momentum and heat
η	variable of integration
$\theta, \tilde{\theta}$	dimensionless temperature
λ	coefficient of friction loss
μ	dynamic viscosity
μ_t	turbulent dynamic viscosity
ν	kinematic viscosity
ξ	variable of integration
ρ	density
τ_{ij}	shear stress
ϕ	coordinate in the tangential direction
$\psi, \tilde{\psi}$	auxiliary function.

pipe. They found that a flow laminarization was set up by an increase in the rotational speed of the pipe if the flow in the pipe is initially turbulent. Additional experiments confirmed the results of the calculations.

Cannon and Kays [11] examined experimentally the effects of tube rotation on the heat transfer to a fluid flowing inside a rotating tube. With an increasing rotational speed a marked decrease of the heat transfer rate could be observed. Visualization experiments showed a strong suppression of the turbulent velocity fluctuations near the rotating tube wall.

The following study will focus attention on the effect of the pipe rotation on the velocity and temperature distribution, on the friction coefficient and on the heat transfer to a fluid flowing inside a rotating pipe. In the experimental investigation great importance is attached to reproducible boundary conditions, i.e. fully developed rotating flow. The analytical study will be performed for flow and heat transfer in an axially rotating pipe by applying a modified mixing length theory to a fully developed turbulent pipe flow with superimposed rotation, as proposed by Kikuyama *et al.* [10] for isothermal flow. To express the degree of turbulence suppression, due to the centrifugal forces, the mixing length will be modified by a function of the Richardson number Ri, proposed by Bradshaw [12].

2. EXPERIMENTS

A schematic outline of the experimental apparatus is shown in Fig. 1. Air was supplied by a centrifugal blower at the end of the rig. In order to obtain fully developed flow conditions, the air was passed through an air filter into the inlet section, which is a non-rotating pipe with an i.d. of $D = 50$ mm and a dimensionless length of $L/D = 50$. The length of the ensuing rotating test section could be varied in the range $0 \leqslant L/D \leqslant 120$. The downstream section of the rotating pipe was heated electrically by means of a slip ring arrangement. At the end of the heated section the rotating tube was separated in two parts by a narrow non-rotating ring of 3 mm length for velocity and temperature measurements. A cylindrical three-hole aerodynamic probe was inserted into the rotating pipe through small holes in the non-rotating ring and traversed in the radial direction, in order to obtain axial and tangential velocity profiles. Temperature profiles could be detected by a traversable thermocouple probe. Behind the non-rotating ring a second rotating

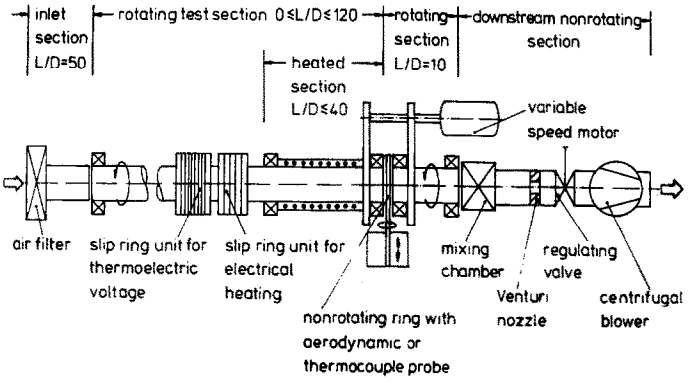

FIG. 1. Experimental apparatus.

pipe section ($L/D = 10$), a mixing chamber for measuring the exit bulk temperature, a downstream nonrotating pipe, a Venturi nozzle for measuring the flow rate and a centrifugal blower were arranged. The rotating tube wall temperature was measured with chromel–alumel thermocouples, which were connected to the instrumentation through a slip ring unit.

To prevent vibrations due to the rotation, the pipe was supported by a series of ball bearings located at intervals of $L/D = 20$. Labyrinth seals were used to prevent leakage between the rotating and the nonrotating parts of the rig. Rotation of the pipes on both sides of the non-rotating ring was accomplished by means of a variable speed d.c. motor and pulley drive. The drive mechanisms provided continuous variation of the rotational speed from 300 to 3000 rev min^{-1}. The flow-rate Reynolds number was varied in the range $5000 \leqslant Re \leqslant 50\,000$ and the rotational Reynolds number in the range $0 \leqslant Re_\phi \leqslant 25\,000$, respectively. Heat transfer coefficients and Nusselt numbers were determined from measurements of the inlet and outlet air temperatures, the wall temperature of the heated section and the mass flow.

3. ANALYSIS

3.1. *The conservation equations in cylindrical coordinates*

In consequence of the steady flow conditions far downstream in the rotating pipe, with constant wall heat flux, all time derivatives become zero. Because of the cylindrical symmetry there are no variations in the tangential direction. For fully developed flow conditions all derivatives in the axial direction are negligible as compared to those in the radial direction, except the pressure gradient and the temperature gradient in the axial direction, which will be constant

$$\frac{\partial}{\partial t} = 0$$

$$\frac{\partial}{\partial \phi} = 0$$

$$\frac{\partial}{\partial z} = 0; \quad \text{except:} \ \frac{\partial p}{\partial z} = \text{const.}; \quad \frac{\partial T}{\partial z} = \text{const.} \qquad (1)$$

Denoting the coordinate system, as illustrated in Fig. 2, by r, ϕ, z as the radial, tangential and axial coordinates, with the corresponding time-smoothed velocities v_r, v_ϕ, v_z and the velocity fluctuations v_r', v_ϕ', v_z', the time-smoothed temperature T and the temperature fluctuation T', the equations of conservation for an incompressible turbulent flow, with negligible body forces acting on the fluid particles except the centrifugal force, without dissipation and with the assumptions made above, take the form:

continuity equation

$$v_r = 0; \qquad (2)$$

radial momentum equation

$$-\rho \frac{v_\phi^2}{r} = -\frac{\partial p}{\partial r} + \frac{1}{r}\frac{\partial}{\partial r}(r\tau_{rr}) - \frac{\tau_{\phi\phi}}{r}; \qquad (3)$$

tangential momentum equation

$$0 = \frac{1}{r^2}\frac{\partial}{\partial r}(r^2\tau_{r\phi}); \qquad (4)$$

axial momentum equation

$$0 = -\frac{\partial p}{\partial z} + \frac{1}{r}\frac{\partial}{\partial r}(r\tau_{rz}); \qquad (5)$$

energy equation

$$\rho c_p v_z \frac{\partial T}{\partial z} = -\frac{1}{r}\frac{\partial}{\partial r}(r\dot{q}_r). \qquad (6)$$

For a newtonian fluid with constant properties the components of the stress tensor can be written as

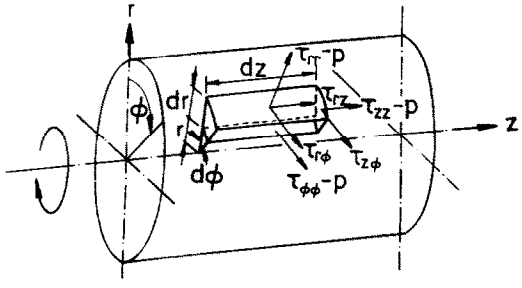

FIG. 2. Cylindrical coordinate system.

$$\tau_{rr} = -\rho\overline{v_r'v_r'}$$

$$\tau_{\phi\phi} = -\rho\overline{v_\phi'v_\phi'}$$

$$\tau_{r\phi} = \mu r\frac{\partial}{\partial r}\left(\frac{v_\phi}{r}\right) - \rho\overline{v_r'v_\phi'}$$

$$\tau_{rz} = \mu\frac{\partial v_z}{\partial r} - \rho\overline{v_z'v_r'}. \tag{7}$$

The radial component of the heat flux vector is

$$\mathring{q}_r = -k\frac{\partial T}{\partial r} + \rho c_p\overline{v_r'T'}. \tag{8}$$

The boundary conditions are

$$r = R:\ v_r = 0;\ v_\phi = v_{\phi w};\ v_z = 0;\ -k\frac{\partial T}{\partial r} = \mathring{q}_{rw}$$

$$r = 0:\ v_r = 0;\ v_\phi = 0;\ \frac{\partial v_z}{\partial r} = 0;\qquad \frac{\partial T}{\partial r} = 0$$

$$z = 0:\ p = p_0;\ T = T_0. \tag{9}$$

In consequence of the assumptions of a constant density fluid with constant properties, the equations of motion and the energy equation are uncoupled and may be solved separately, since the inaccuracy is less than 5% for a wall to fluid bulk temperature ratio $T_w/T_B = 1.2$, as can be proved. Therefore, the momentum equation will be considered first, in order to calculate the velocity profile and the friction factor.

3.2. *Velocity distribution and friction coefficient*

Integration of the axial momentum equation (5) yields a correlation between the shear stress τ_{rz} and the axial pressure gradient

$$\tau_{rz} = \frac{r}{2}\frac{\partial p}{\partial z}. \tag{10}$$

Introducing the friction coefficient of the pipe, λ, the pressure gradient along the pipe can be expressed as

$$\frac{\partial p}{\partial z} = -\frac{\lambda}{R}\frac{\rho}{4}\bar{v}_z^2 \tag{11}$$

with the mean axial velocity

$$\bar{v}_z = \frac{\int_{r=0}^{R} v_z r\,\mathrm{d}r}{\int_{r=0}^{R} r\,\mathrm{d}r}. \tag{12}$$

Elimination of the axial pressure gradient in equations (10) and (11) yields

$$\tau_{rz} = -\frac{\lambda}{8}\frac{r}{R}\rho\bar{v}_z^2. \tag{13}$$

The shear stress at the pipe wall ($r = R$) becomes

$$\tau_{rz,w} = -\frac{\lambda}{8}\rho\bar{v}_z^2. \tag{14}$$

3.2.1. *The turbulence model.* Using Prandtl's modified mixing length theory, as proposed by Koosinlin *et al.* [13], the axial shear stress τ_{rz} in equation (13) can be written as

$$\tau_{rz} = \left[\mu + \rho l^2\left(\left[\frac{\partial v_z}{\partial r}\right]^2 + \left[r\frac{\partial}{\partial r}\left(\frac{v_\phi}{r}\right)\right]^2\right)^{1/2}\right]\frac{\partial v_z}{\partial r} \tag{15}$$

where l is the mixing length. Substituting equation (13) into equation (15), we obtain

$$l^2\left(\left[\frac{\partial v_z}{\partial r}\right]^2 + \left[r\frac{\partial}{\partial r}\left(\frac{v_\phi}{r}\right)\right]^2\right)^{1/2}\frac{\partial v_z}{\partial r} + \nu\frac{\partial v_z}{\partial r} + \frac{\lambda}{8}\frac{r}{R}\bar{v}_z^2 = 0. \tag{16}$$

A common correlation between the mixing length in a non-rotating pipe l_0 and the radial coordinate r is Nikuradse's mixing length expression [14]

$$\frac{l_0}{R} = 0.14 - 0.08\left(\frac{r}{R}\right)^2 - 0.06\left(\frac{r}{R}\right)^4. \tag{17}$$

Near the tube wall, in the viscous sublayer, the mixing length becomes zero, and equation (17), therefore, must be multiplied by van Driest's damping factor

$$1 - \mathrm{e}^{-y^+/26} \tag{18}$$

with the dimensionless distance from the wall

$$y^+ = \frac{v_*(R-r)}{\nu}. \tag{19}$$

Here

$$v_* = \sqrt{\left(\frac{|\tau_{rz,w}|}{\rho}\right)} \tag{20}$$

is the friction velocity. The mixing length l_0 now can be expressed as

$$\frac{l_0}{R} = [1 - \mathrm{e}^{-y^+/26}]\left[0.14 - 0.08\left(\frac{r}{R}\right)^2 - 0.06\left(\frac{r}{R}\right)^4\right]. \tag{21}$$

In a rotating system the turbulence, i.e. the mixing length l, is markedly effected by the centrifugal force. To describe the suppression of turbulence with radially growing centrifugal forces, the mixing length l_0 in equation (21) must be modified for the flow in a rotating tube. Bradshaw [12] proposed the following equation:

$$\frac{l}{l_0} = (1 - \beta Ri)^\alpha \tag{22}$$

where α and β are constants and Ri the Richardson number, defined by

$$Ri = \frac{2\frac{v_\phi}{r^2}\frac{\partial}{\partial r}(v_\phi r)}{\left[\frac{\partial v_z}{\partial r}\right]^2 + \left[r\frac{\partial}{\partial r}\left(\frac{v_\phi}{r}\right)\right]^2}. \tag{23}$$

Without rotation, $Ri = 0$, there exists a fully turbulent pipe flow. If $Ri > 0$, i.e. for a rotating tube with a radially growing tangential velocity, the centrifugal forces suppress the turbulent fluctuations and the mixing length decreases. If $Ri < 0$, e.g. for flows over spinning surfaces, turbulence increases.

According to experiments in refs. [10, 15], the profile of the tangential velocity $v_\phi(r)$ in the fully developed flow region ($L_{rot}/D \geqslant 120$) may be characterized by a parabolic distribution as expressed by

$$v_\phi = \left(\frac{r}{R}\right)^2 v_{\phi w}. \tag{24}$$

Introducing the dimensionless radius $\tilde{r} = r/R$, the dimensionless axial velocity $\tilde{v}_z = v_z/v_*$, the flow-rate Reynolds number

$$Re = \frac{\bar{v}_z D}{\nu} \tag{25}$$

the rotational Reynolds number

$$Re_\phi = \frac{v_{\phi w} D}{\nu} \tag{26}$$

the rotation rate

$$N = \frac{v_{\phi w}}{\bar{v}_z} = \frac{Re_\phi}{Re} \tag{27}$$

and the tangential velocity profile, defined by equation (24), results in the following expression for the Richardson number:

$$Ri = \frac{6\tilde{r}^2 N^2}{\left[\dfrac{\partial}{\partial r}\left(\dfrac{v_z}{\bar{v}_z}\right)\right]^2 + \tilde{r}^2 N^2}. \tag{28}$$

With increasing rotation rate $N \to \infty$, the Richardson number will approach the boundary value $Ri = 6$. Therefore, the constant β in equation (22) will be $\beta = 1/6$. Matching the theory with the experiments results in $\alpha = 2$, and l/l_0 yields

$$\frac{l}{l_0} = \left(1 - \frac{1}{6} Ri\right)^2. \tag{29}$$

3.2.2. *Solution of the momentum equation.* From equations (20) and (14) the shear velocity can be expressed as

$$v_* = \sqrt{\left(\frac{\lambda}{8}\right)} \bar{v}_z. \tag{30}$$

With this, the friction coefficient λ in equation (16) can be substituted by the friction velocity v_*. Utilizing equations (24)–(27) and

$$Re_* = \frac{v_* R}{\nu} \tag{31}$$

the Reynolds number defined with the friction velocity v_*, equation (16) can be transformed into dimensionless form

$$\left(\frac{l}{R}\right)^2 \left[1 + \left[\frac{\tilde{r} N \dfrac{Re}{2Re_*}}{\dfrac{d\tilde{v}_z}{d\tilde{r}}}\right]^2\right]^{1/2} \left(\frac{d\tilde{v}_z}{d\tilde{r}}\right)^2 - \frac{1}{Re_*}\frac{d\tilde{v}_z}{d\tilde{r}} - \tilde{r} = 0. \tag{32}$$

In equation (32) the partial differentials are replaced by total differentials, since the velocity $\tilde{v}_z$ is only a function of the radial coordinate $\tilde{r}$. With l/R from equations (21), (28) and (29), the gradient of the axial velocity $d\tilde{v}_z/d\tilde{r}$ can be calculated numerically by equation (32) at any radial position with an assumed value of Re_* corresponding to the given values of Re and N. Numerical integration of the velocity gradient yields the dimensionless axial velocity

$$\tilde{v}_z(\tilde{r}) = \int_{\tilde{r}=1}^{\tilde{r}} \left(\frac{d\tilde{v}_z}{d\tilde{r}}\right) d\tilde{r}. \tag{33}$$

The dimensionless axial mean velocity $\bar{\tilde{v}}_z$ can be calculated by a second integration

$$\bar{\tilde{v}}_z = \frac{\bar{v}_z}{v_*} = 2\int_{\tilde{r}=0}^{1} \tilde{v}_z \tilde{r}\, d\tilde{r}. \tag{34}$$

With equations (25) and (31) the flow-rate Reynolds number can be determined as

$$Re = 2Re_* \bar{\tilde{v}}_z. \tag{35}$$

If Re (equation (35)) deviates more than $\varepsilon \leqslant 10^{-4}$ from the initial value, the calculation is repeated with a corrected value of Re_* until $\varepsilon \leqslant 10^{-4}$ is satisfied. With the calculated velocity distribution, profiles of the Richardson number Ri and the mixing length l/R can be obtained by equation (28) or equations (29) and (21), respectively. Utilizing equations (30) and (34) the friction factor λ becomes

$$\lambda = \frac{8}{\bar{\tilde{v}}_z^2}. \tag{36}$$

3.3. *Temperature distribution and Nusselt number*

As the heat transfer in the region of fully developed thermal conditions is to be considered, it is apparent that the last boundary condition ($T = T_0$ at $z = 0$; equation (9)) for the energy equation cannot be satisfied. Hence we replace the latter by

$$-2\pi R z \dot{q}_{rw} = \int_{\phi=0}^{2\pi} \int_{r=0}^{R} \rho c_p (T - T_0) v_z r\, dr\, d\phi. \tag{37}$$

For the solution of the energy equation (6) a turbulence hypothesis is required, that combines the turbulent energy flux with the mean velocities. Since the mechanisms of momentum and energy transport in a turbulent flow are very similar, an adaption of Prandtl's mixing length hypothesis to the heat transfer is suitable. In analogy to equation (15) we can write for the radial heat flux

$$\mathring{q}_r = \left[-k - \rho c_p l l_q \left(\left[\frac{\partial v_z}{\partial r} \right]^2 + \left[r \frac{\partial}{\partial r} \left(\frac{v_\phi}{r} \right) \right]^2 \right)^{1/2} \right] \frac{\partial T}{\partial r} \tag{38}$$

where l_q denotes the thermal mixing length. The influence of the centrifugal forces on the thermal mixing length is expressed by the same equation as the influence on the hydrodynamic mixing length

$$\frac{l_q}{l_{q0}} = \left(1 - \frac{1}{6} Ri \right)^2. \tag{39}$$

The ratio of the hydrodynamic mixing length l_0 and the thermal mixing length l_{q0} or the ratio of the turbulent diffusivities of momentum ε_τ and heat ε_q, respectively, is referred to the literature as the turbulent Prandtl number

$$Pr_t = \frac{\varepsilon_\tau}{\varepsilon_q} = \frac{l_0}{l_{q0}} = \frac{\overline{v_r' v_z'}}{\overline{v_r' T'}} \frac{\overline{\partial T}}{\overline{\partial r}} \frac{\overline{\partial v_z}}{\overline{\partial r}}. \tag{40}$$

In an experimental investigation of turbulent pipe flow performed by Ludwicg [16] it was found, that the ratio $l_{q0}/l_0 = 1/Pr_t$ varies from about 1 at the wall to about 1.5 in the centre of the pipe. These results can be expressed by the empirical equation

$$\frac{1}{Pr_t} = \frac{l_{q0}}{l_0} = 1.53 - 2.82\tilde{r}^2 + 3.85\tilde{r}^3 - 1.48\tilde{r}^4. \tag{41}$$

To simplify manipulations, we introduce the following dimensionless quantities:

$$\theta = \frac{T - T_0}{\frac{\mathring{q}_{rw} R}{k}} \tag{42}$$

$$\tilde{z} = \frac{zk}{\rho c_p v_* R^2} = \frac{z}{R} \frac{1}{Re_* Pr}. \tag{43}$$

With this and with equation (38), the energy equation (6) can be written as

$$\tilde{v}_z \frac{\partial \theta}{\partial \tilde{z}} = \frac{1}{\tilde{r}} \frac{\partial}{\partial \tilde{r}} \left(\left[1 + Pr\, Re_* \frac{l}{R} \frac{l_q}{R} \left(\left[\frac{\partial \tilde{v}_z}{\partial \tilde{r}} \right]^2 + \left[\tilde{r} N \frac{Re}{2Re_*} \right]^2 \right)^{1/2} \right] \tilde{r} \frac{\partial \theta}{\partial \tilde{r}} \right). \tag{44}$$

As fully developed thermal conditions are considered, a constant wall heat flux will result in a fluid temperature increase which is linear in the $\tilde{z}$-direction. One further expects that the shape of the radial temperature profiles will ultimately not undergo further change with increasing $\tilde{z}$. Hence a solution of the following form seems reasonable for large values of $\tilde{z}$:

$$\theta(\tilde{r}, \tilde{z}) = C_1 \tilde{z} + \psi(\tilde{r}). \tag{45}$$

Substituting equation (45) into equation (44) gives the following ordinary differential equation for $\psi(\tilde{r})$:

$$\tilde{v}_z(\tilde{r}) C_1 = \frac{1}{\tilde{r}} \frac{\mathrm{d}}{\mathrm{d}\tilde{r}} \left[F(\tilde{r}) \tilde{r} \frac{\mathrm{d}\psi(\tilde{r})}{\mathrm{d}\tilde{r}} \right] \tag{46}$$

where

$$F(\tilde{r}) = 1 + \frac{k_\tau}{k} = 1 + Pr\, Re_* \frac{l}{R} \frac{l_q}{R} \left(\left[\frac{\partial \tilde{v}_z}{\partial \tilde{r}} \right]^2 + \left[\tilde{r} N \frac{Re}{2Re_*} \right]^2 \right)^{1/2}. \tag{47}$$

This equation is integrated twice, with respect to $\tilde{r}$, to give

$$\psi(\tilde{r}) = C_1 \int_{\eta=0}^{\tilde{r}} \left[\frac{1}{F(\eta)\eta} \int_{\xi=0}^{\eta} \tilde{v}_z(\xi) \xi \, \mathrm{d}\xi \right] \mathrm{d}\eta + C_2 \int_{\xi=0}^{\tilde{r}} \frac{1}{F(\xi)\xi} \mathrm{d}\xi + C_3. \tag{48}$$

The constants of integration, C_1 and C_2, are determined with the aid of the boundary conditions (equation (9)) to be

$$C_2 = 0$$

$$C_1 = -4 \frac{Re_*}{Re}. \tag{49}$$

Substitution of equations (48) and (49) into equation (45) gives

$$\theta(\tilde{r}, \tilde{z}) = -4 \frac{Re_*}{Re} \tilde{z} - 4 \frac{Re_*}{Re} \times \int_{\eta=0}^{\tilde{r}} \left[\frac{1}{F(\eta)\eta} \int_{\xi=0}^{\eta} \tilde{v}_z(\xi) \xi \, \mathrm{d}\xi \right] \mathrm{d}\eta + C_3 = -4 \frac{Re_*}{Re} \tilde{z} + \bar{\psi}(\tilde{r}) + C_3. \tag{50}$$

Substituting this temperature function into equation (37) yields

$$C_3 = -4 \frac{Re_*}{Re} \int_{\tilde{r}=0}^{1} \bar{\psi}(\tilde{r}) \tilde{v}_z(\tilde{r}) \tilde{r} \, \mathrm{d}\tilde{r}. \tag{51}$$

With this, the temperature distribution is finally given by

$$\theta(\tilde{r}, \tilde{z}) = -4 \frac{Re_*}{Re} \tilde{z} + \bar{\psi}(\tilde{r}) - 4 \frac{Re_*}{Re} \int_{\tilde{r}=0}^{1} \bar{\psi}(\tilde{r}) \tilde{v}_z(\tilde{r}) \tilde{r} \, \mathrm{d}\tilde{r} \tag{52}$$

where $\bar{\psi}(\tilde{r})$ is defined by equation (50). With the velocity distribution, calculated in Section 3.2, and using equations (47), (39), (40) and (21), the temperature profile in the rotating tube is obtained.

The heat transfer coefficient is determined from the temperature gradient at the wall. For the Nusselt number based on the local difference between the wall

temperature and the fluid bulk temperature

$$\theta_B(\tilde{z}) = \frac{\int_{\tilde{r}=0}^{1} \theta(\tilde{r},\tilde{z})\tilde{v}_z(\tilde{r})\tilde{r}\,d\tilde{r}}{\int_{\tilde{r}=0}^{1} \tilde{v}_z(\tilde{r})\tilde{r}\,d\tilde{r}} \tag{53}$$

we can write

$$Nu = \frac{2\left.\frac{\partial\theta}{\partial\tilde{r}}\right|_{\tilde{r}=1}}{\theta(1,\tilde{z}) - \theta_B(\tilde{z})}. \tag{54}$$

The introduction of equation (52) and the boundary conditions (equation (9)) yields

$$Nu = \frac{-2}{\bar{\psi}(1) + C_3} \tag{55}$$

where $\bar{\psi}(1)$ and C_3 are given by equations (50) and (51), respectively.

4. RESULTS AND DISCUSSION

4.1. *Velocity distribution*

The effects of the rotation rate N on the axial and tangential velocity distribution for fully developed flow conditions are shown in Figs. 3 and 4 for different flow-rate Reynolds numbers. The experimental results

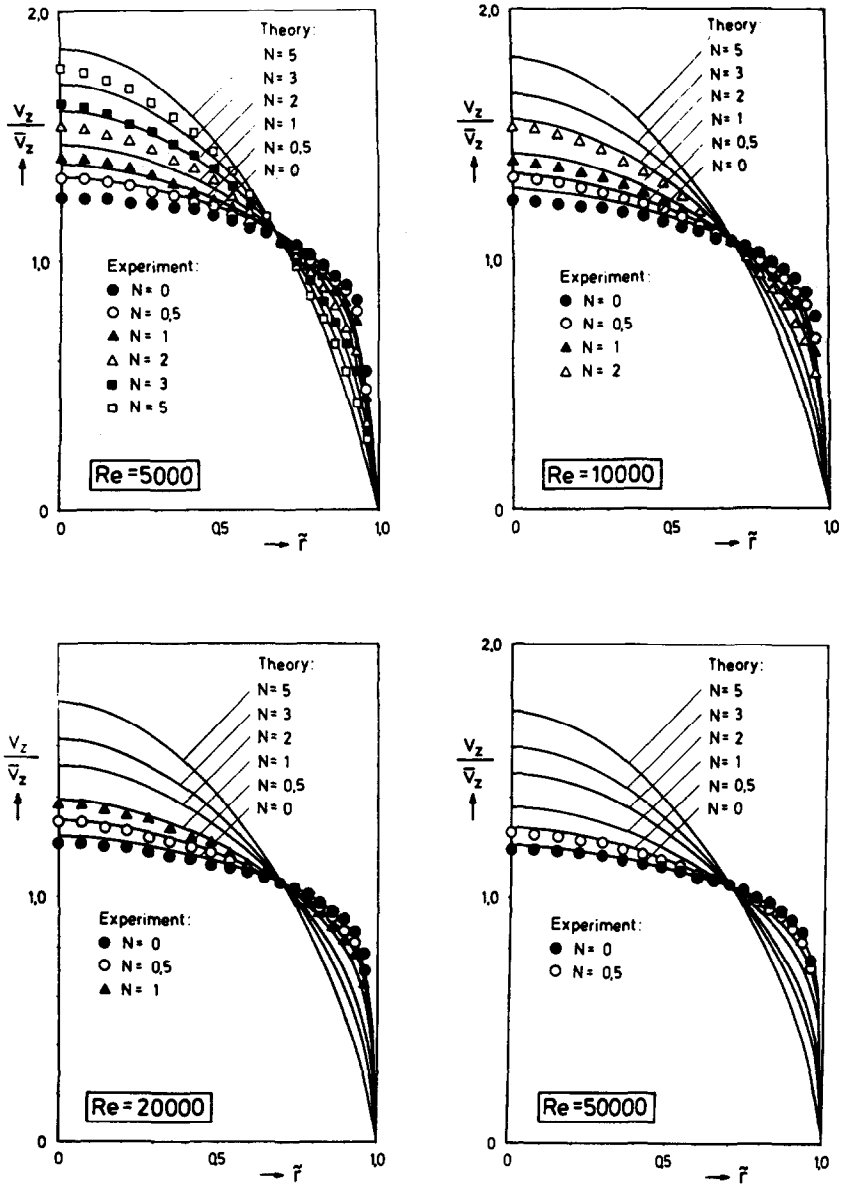

FIG. 3. Axial velocity distribution as a function of the rotation rate N.

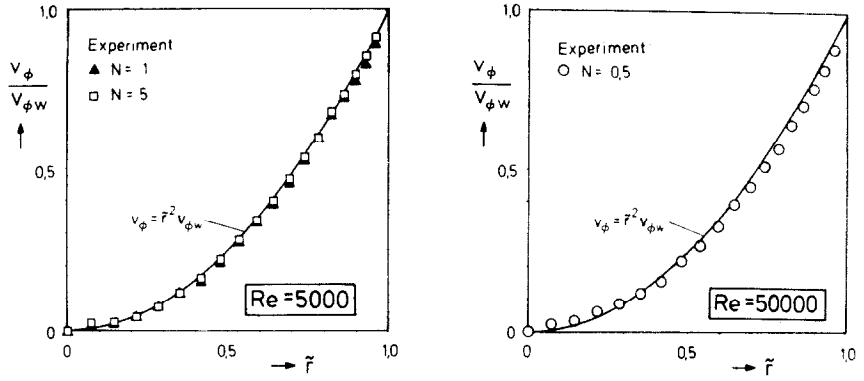

FIG. 4. Tangential velocity distribution as a function of the rotation rate N.

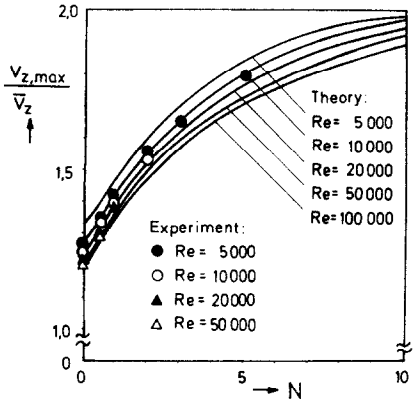

FIG. 5. Ratio of the maximum to the mean axial velocity as a function of the rotation rate N.

are plotted for comparison. The validity of the assumption for the tangential velocity profile (equation (24)) is well confirmed by the experiments. Generally the calculated profiles of the axial velocity are in good agreement with the experiments. For $Re = 5000$, however, the measured velocities deviate slightly from the theoretical result. With increasing rotation rate N the axial velocity profiles gradually approach the parabolic shape of the Hagen–Poiseuille flow which corresponds to increasing turbulence suppression due to pipe rotation.

In Fig. 5 the ratio of the maximum axial velocity in the tube centre and the mean axial velocity $v_{z,\max}/\bar{v}_z$ is plotted vs the rotation rate N. With increasing N the values of $v_{z,\max}/\bar{v}_z$ grow and approach asymptotically the value of 2, which is valid for laminar tube flow.

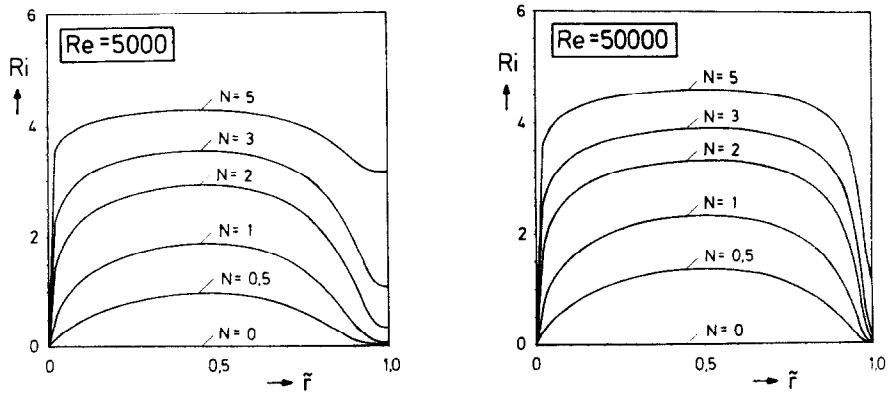

FIG. 6. The Richardson number Ri as a function of the rotation rate N.

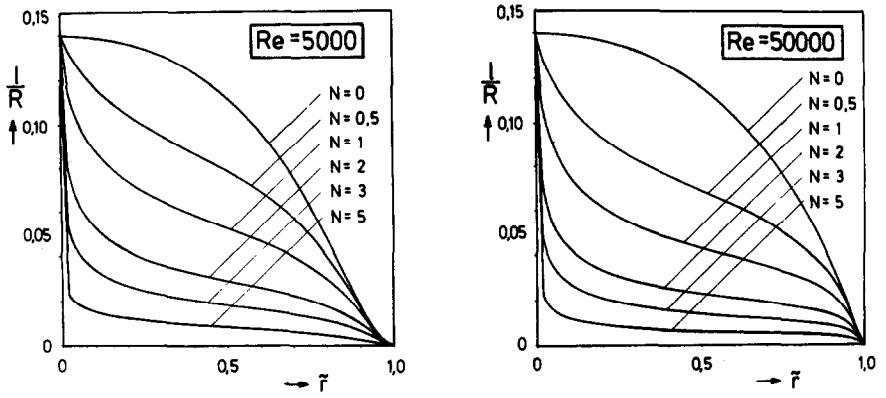

FIG. 7. The mixing length l as a function of the rotation rate N.

4.2. *Richardson number and mixing length*

To illustrate the effect of turbulence suppression due to pipe rotation, distributions of the Richardson number (equation (28)) and the mixing length are depicted in Figs. 6 and 7, respectively. In the tube centre, at $\tilde{r} = 0$, the Richardson number is zero, near the pipe wall, at $\tilde{r} = 1$, the Richardson number approaches a constant value, that is growing with the rotation rate N. The maximum value of the Richardson number is registered at $\tilde{r} \approx 0.5$. Hence, in this region, the turbulence suppression is most pronounced. The value of the maximum Richardson number is growing with increasing rotation rate N.

Figure 7 shows the influence of the tube rotation on the mixing length l. For turbulent pipe flow without rotation, the mixing length distribution is that given by Nikuradse with the van Driest damping factor (equation (21)). The mixing length distribution in the rotating tube, obtained from equations (21) and (29), elucidates the turbulence suppression with growing rotation rate N. The suppression is most pronounced at $\tilde{r} \approx 0.5$, as predicted by the Richardson number distribution.

4.3. *The friction coefficient*

In Fig. 8 the friction factor λ is plotted against the flow-rate Reynolds number Re for various values of the rotation rate N. A remarkable decrease in λ can be observed with increasing N. For $N \to 0$ the friction coefficient is that predicted by the Blasius resistance formula, $\lambda = 0.3164 Re^{-0.25}$.

In contrast to Fig. 8, the influence of the rotational Reynolds number Re_ϕ on the friction factor is visualized in Fig. 9. For constant Re_ϕ the pressure loss shifts towards that of the non-rotating pipe with increasing flow-rate Reynolds number. Hence, the influence of rotation on the pressure loss decreases with an increasing flow rate. For a decreasing flow rate, the friction coefficient approaches gradually that of the laminar pipe flow, $\lambda = 64/Re$.

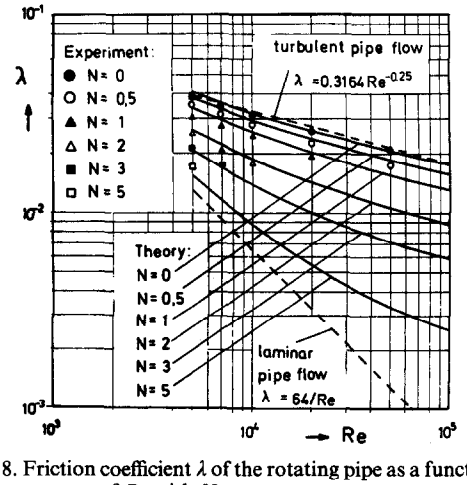

FIG. 8. Friction coefficient λ of the rotating pipe as a function of Re with N as a parameter.

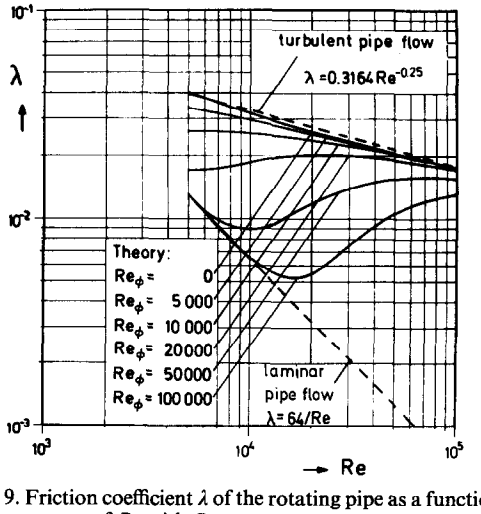

FIG. 9. Friction coefficient λ of the rotating pipe as a function of Re with Re_ϕ as a parameter.

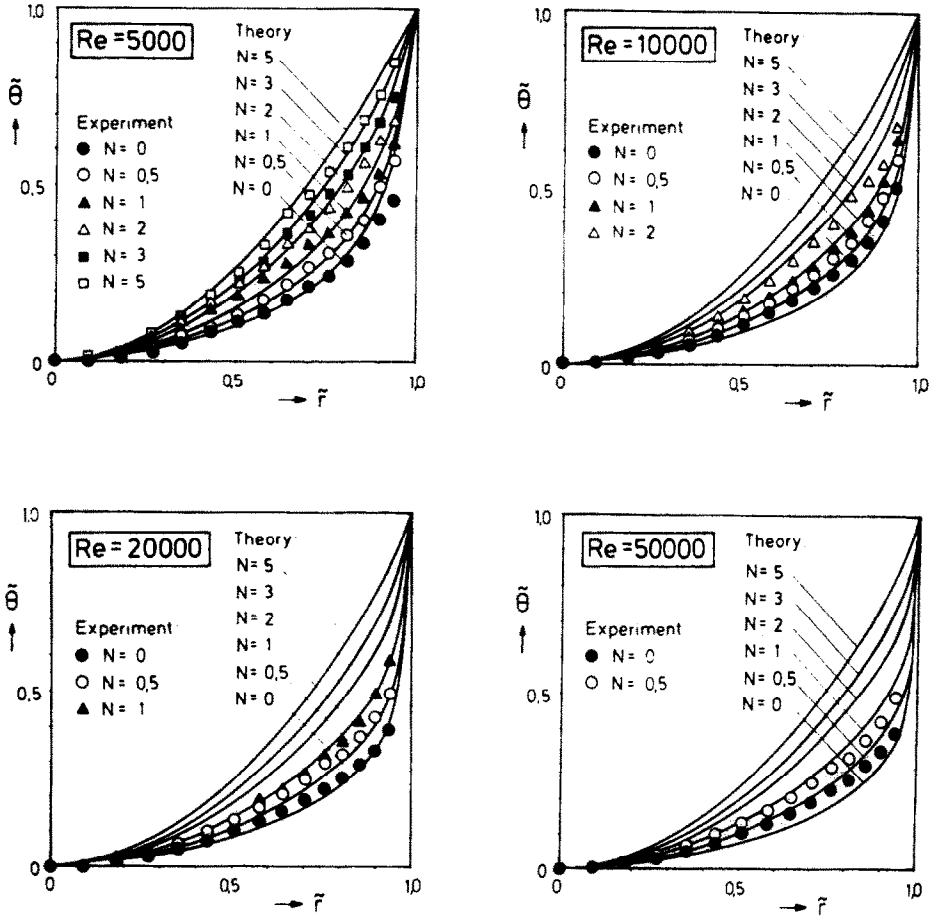

FIG. 10. Temperature distribution as a function of the rotation rate N $[\tilde{\theta} = (T(\tilde{r}) - T(\tilde{r} = 0))/(T(\tilde{r} = 1) - T(\tilde{r} = 0))]$.

4.4. *Temperature distribution*

The influence of the rotation rate N on the temperature distribution for fully developed hydrodynamic and thermal boundary layers is depicted in Fig. 10. The experimental results are in close agreement with the theoretical predictions, calculated by equation (52). With an increasing rotation rate the temperature profiles shift towards that for the laminar pipe flow, which is a consequence of turbulence suppression.

4.5. *The Nusselt number*

In Fig. 11 the Nusselt number Nu is plotted as a function of the flow-rate Reynolds number Re for various values of the rotation rate N. For $N = 0$, i.e. for turbulent pipe flow without rotation, the curve of the Nusselt number is in good agreement with that of Reynolds' analogy, $Nu = 0.04(Re\,Pr)^{0.75}$. With an increase in N a remarkable decrease in the Nusselt number can be observed. The experimental results are in close agreement with the theory, except for very low Reynolds numbers ($Re = 5000$).

Figure 12 shows the Nusselt number Nu as a function of the flow-rate Reynolds number Re, with the rotational Reynolds number Re_ϕ as a parameter. In this plot the influence of the flow-rate Reynolds number on the Nusselt number for the flow inside a tube, rotating with a constant number of revolutions, is

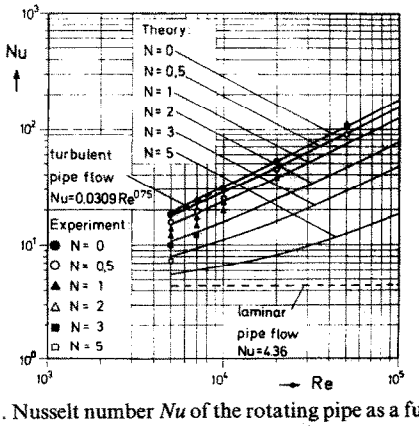

FIG. 11. Nusselt number Nu of the rotating pipe as a function of Re with N as a parameter.

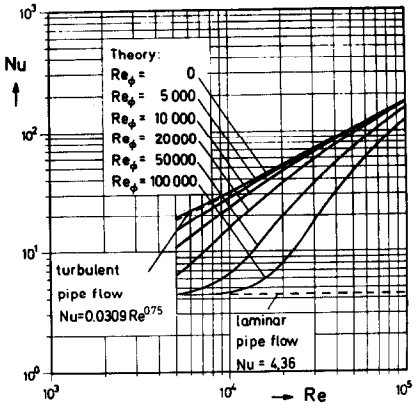

FIG. 12. Nusselt number Nu of the rotating pipe as a function of Re with Re_ϕ as a parameter.

demonstrated. For constant Re_ϕ the Nusselt number approaches that for the non-rotating pipe with an increasing flow-rate Reynolds number. For a decreasing flow rate the effect of rotation becomes more pronounced and the Nusselt number approaches gradually the value for the laminar pipe flow, $Nu = 4.36$.

5. CONCLUSIONS

Experiments and calculations were performed for fluid flow and heat transfer in an axially rotating tube for fully developed hydrodynamic and thermal boundary layers. In the analytical study a modified mixing length hypothesis, which takes into account turbulence suppression due to the centrifugal forces, was applied. There is a good agreement between experimental findings and theoretical results.

The tube rotation apparently effects a suppression of the turbulent motion. Measured and calculated velocity and temperature profiles reveal a pronounced flow laminarization. At turbulent flow-rate Reynolds numbers the flow resistance and the heat transfer is considerably reduced by the pipe rotation. This is caused by a suppression of the radial turbulent migration of fluid particles due to the radially growing centrifugal forces which is demonstrated by the mixing length distribution for different rotation rates.

Acknowledgement—The support of this work by the Deutsche Forschungsgemeinschaft is greatly acknowledged.

REFERENCES

1. Lord Rayleigh, On the dynamics of revolving fluids, *Proc. R. Soc.* **A93,** 148–154 (1917).
2. T. von Kármán, Über laminare und turbulente Reibung, *Z. Angew. Math. Mech.* **1,** 233–251 (1921).
3. G. I. Taylor, Stability of a viscous liquid contained between two rotating cylinders, *Phil. Trans. R. Soc. (London)* **A223,** 289–343 (1923).
4. F. Levy, Strömungserscheinungen in rotierenden Rohren, *VDI ForschArb. Geb. IngWes.* **322,** 18–45 (1929).
5. A. White, Flow of fluid in an axially rotating pipe, *J. Mech. Engng Sci.* **6,** 47–52 (1964).
6. V. K. Shchukin, Hydraulic resistance of rotating tubes, *J. Engng Phys.* **12,** 418–422 (1967).
7. A. I. Borisenko, O. N. Kostikov and V. I. Chumachenko, Experimental study of turbulent flow in a rotating channel, *J. Engng Phys.* **24,** 770–773 (1973).
8. M. Murakami and K. Kikuyama, Turbulent flow in axially rotating pipes, *J. Fluids Engng* **102,** 97–103 (1980).
9. K. Kikuyama, M. Murakami and K. Nishibori, Development of three-dimensional turbulent boundary layer in an axially rotating pipe, *J. Fluids Engng* **105,** 154–160 (1983).
10. K. Kikuyama, M. Murakami, K. Nishibori and K. Maeda, Flow in an axially rotating pipe, *Bull. J.S.M.E.* **26,** 506–513 (1983).
11. J. N. Cannon and W. M. Kays, Heat transfer to a fluid flowing inside a pipe rotating about its longitudinal axis, *J. Heat Transfer* **91,** 135–139 (1969).
12. P. Bradshaw, The analogy between streamline curvature and buoyancy in turbulent shear flow, *J. Fluid Mech.* **36,** 177–191 (1969).
13. M. L. Koosinlin, B. E. Launder and B. I. Sharma, Prediction of momentum, heat and mass transfer in swirling, turbulent boundary layers, *J. Heat Transfer* **96,** 204–209 (1975).
14. H. Schlichting, *Boundary Layer Theory* (7th Edn). McGraw-Hill, New York (1979).
15. G. Reich, Strömung und Wärmeübertragung in einem axial rotierenden Rohr, Doctoral Thesis, TH Darmstadt (1988).
16. H. Ludwieg, Bestimmung des Verhältnisses der Austauschkoeffizienten für Wärme und Impuls bei turbulenten Grenzschichten, *Z. Flugwiss.* **4,** 73–81 (1956).
17. K. Nishibori, K. Kikuyama and M. Murakami, Laminarization of turbulent flow in the inlet region of an axially rotating pipe, *Bull. J.S.M.E.* **30,** 255–260 (1987).

ECOULEMENT ET TRANSFER DE CHALEUR DANS UN TUBE EN ROTATION—I. EFFET DE LA ROTATION SUR UN ECOULEMENT TURBULENT EN CONDUITE CYLINDRIQUE

Résumé—Les effets de la rotation d'un tube horizontal sur la distribution de vitesse et de température ainsi que sur le coefficient de frottement et le transfert de chaleur d'un écoulement axial turbulent sont étudiés expérimentalement et analytiquement. Nous montrons que la rotation du tube et ainsi la présence de forces centrifuges croissant radialement a un important effet sur la diminution de la turbulence. L'étude analytique de l'écoulement et du transfert de chaleur dans un tube horizontal en rotation se base sur la théorie d'une longueur de mélange modifiée d'un écoulement turbulent établi en conduite cylindrique avec rotation superposée. Pour exprimer le degré de diminution de la turbulence due aux forces centrifuges, la longueur de mélange est modifiée par une fonction du nombre de Richardson Ri. Les résultats théoriques sont comparés aux résultats expérimentaux.

STRÖMUNG UND WÄRMEÜBERTRAGUNG IN EINEM AXIAL ROTIERENDEN ROHR—I. EINFLUSS DER ROTATION AUF EINE TURBULENTE ROHRSTRÖMUNG

Zusammenfassung—Der Einfluß der Rotation auf Geschwindigkeits- und Temperaturprofile, Reibungsbeiwert und Wärmeübergangszahl einer turbulenten Rohrströmung wird experimentell und theoretisch untersucht. Es wird gezeigt, daß die Rotation aufgrund der radial ansteigenden Zentrifugalkräfte einen ausgeprägten Einfluß auf die Unterdrückung der turbulenten Bewegung hat. Mittels einer modifizierten Mischungswegtheorie für die voll ausgebildete turbulente Rohrströmung mit überlagerter Rotation wird eine analytische Untersuchung der Strömung und der Wärmeübertragung in einem axial rotierenden Rohr durchgeführt. Um den Grad der Turbulenzunterdrückung aufgrund der Zentrifugalkräfte darzustellen, wird der Mischungsweg mit einer Funktion der Richardsonzahl *Ri* modifiziert. Die theoretischen Ergebnisse werden mit den experimentellen Befunden verglichen.

ТЕЧЕНИЕ ЖИДКОСТИ И ТЕПЛОПЕРЕНОС В АКСИАЛЬНО ВРАЩАЮЩЕЙСЯ ТРУБЕ—I. ВЛИЯНИЕ ВРАЩЕНИЯ НА ТРУБУЛЕНТНОЕ ТЕЧЕНИЕ В ТРУБЕ

Аннотация—Экспериментально и аналитически исследуется влияние вращения трубы на распределения скоростей и температур, на коэффициент трения и на теплоперенос в потоке жидкости в трубе. Найдено, что вращение очень сильно подавляет турбулентность в силу возрастающих в радиальном направлении центробежных сил. С использованием модифицированной теории пути смешения для полностью развитого течения во вращающейся трубе проведено аналитическое исследование течения и теплопереноса. Для учета степени подавления турбулентности центробежными силами величина пути смешения модифицируется как функция числа Ричардсона *Ri*. Теоретические результаты сравниваются с экспериментальными данными.